Marine Pollution Bulletin 60 (2010) 1412–1422

Contents lists available at ScienceDirect

Marine Pollution Bulletin

journal homepage: www.elsevier.com/locate/marpolbul

A set of rapid-response models for pollutant dispersion assessments in southern Spain coastal waters

R. Periáñez [a,*], F. Caravaca [b]

[a] Dpto. Física Aplicada I, E.U. Ingeniería Técnica Agrícola, Universidad de Sevilla. Ctra. Utrera km 1, 41013-Sevilla, Spain
[b] Dpto. Ciencias Agroforestales, E.U. Ingeniería Técnica Agrícola, Universidad de Sevilla. Ctra. Utrera km 1, 41013-Sevilla, Spain

ARTICLE INFO

Keywords:
Numerical modelling
Pollutant spill
Particle-tracking
Hydrodynamics
Alborán Sea
Gulf of Cádiz
Gibraltar Strait

ABSTRACT

Three rapid-response Lagrangian particle-tracking dispersion models have been developed for southern Spain coastal waters. The three domains cover the Gulf of Cádiz (Atlantic Ocean), the Alborán Sea (Mediterranean), and the Strait of Gibraltar with higher spatial resolution. The models are based on different hydrodynamic submodels, which are run in advance. Tides are calculated using a 2D barotropic model in the three cases. Models used to obtain the residual circulation depend on the physical oceanography of each region. Thus, two-layer models are applied to Gibraltar Strait and Alborán Sea and a 3D baroclinic model is used in the Gulf of Cádiz. Results from these models have been compared with observations to validate them and are then used by the particle-tracking models to calculate dispersion. Chemical, radioactive and oil spills may be simulated, incorporating specific processes for each kind of pollutant. Several application examples are provided.

1. Introduction

Recently, there has been an increasing interest in the development of pollutant dispersion models for the marine environment to be used for decision making purposes after contaminant spills. In particular, particle-tracking methods are well suited for problems in which high contamination gradients are involved, since they minimize the effects of numerical diffusion. Also, they can be used to rapidly assess contaminant dispersion if the hydrodynamics are simulated previously off-line. Particle-tracking models have been used to simulate the dispersion of passive tracers (Harms et al., 2000; Gomez-Gesteira et al., 1999), radionuclides (Schonfeld, 1995; Periáñez and Elliott, 2002; Kobayashi et al., 2007), chemicals (Havens et al., 2009) and oil spills (Proctor et al., 1994; Korotenko et al., 2004) in several coastal water environments.

The *Prestige* tanker oil spill, occurred in November 2002 off the northwest Spanish coast, highlighted the limitations of the Spanish operational oceanography capability to respond to an emergency situation of this nature. Consequently, some efforts have been undertaken since then. Carracedo et al. (2006) have developed an operational oceanography system for the northwest of Spain, which was applied to hindcast oil trajectories after the Prestige spill. Similar systems have also been developed for the northern Spanish coast (Cantabric Sea) by Sotillo et al. (2008) and for the east coast (Mediterranean Sea) by Jordi et al. (2006). All these models are based upon particle-tracking methods.

The Strait of Gibraltar (GS) connects the Gulf of Cádiz (GoC), in the Atlantic Ocean, with the Alborán Sea (AS), in the western Mediterranean. This is an intense traffic zone for oil tankers, allowing to access to Southern Europe, North Africa, the Middle East and the Black Sea. Indeed, there is a traffic over 70,000 merchant vessels per year, 30% of them declaring hazardous cargos between the Atlantic and the Mediterranean. Traffic of oil tankers is about 5000 vessels per year (Nav42, 1998). Transit of nuclear submarines and of vessels transporting radioactive waste must also be considered.

The objective of this paper consists of describing a set of models which predict oil and chemical spill trajectories in southern Spain coastal waters. These models are essential to adequately manage response after an emergency situation in coastal waters. Only some initial developments have been carried out until now for these waters. Thus, Periáñez (2007) and Periáñez and Pascual-Granged (2008) have described particle-tracking models for the AS and GS, respectively, but they could only be applied in the case of a pollutant spill occurring at the sea surface. Now, fully 3D dispersion models, which may simulate a pollutant release occurring at any depth, have been developed for three spatial domains: GoC, AS and a higher resolution model of GS. These spatial domains are shown in Fig. 1. The models are based upon hydrodynamic models which run off-line and provide tidal and residual circulations in each domain. These are stored in files which will be read by the dispersion code to obtain water current at any time and position.

* Corresponding author.
E-mail address: rperianez@us.es (R. Periáñez).

0025-326X/$ - see front matter © 2010 Elsevier Ltd. All rights reserved.
doi:10.1016/j.marpolbul.2010.05.016

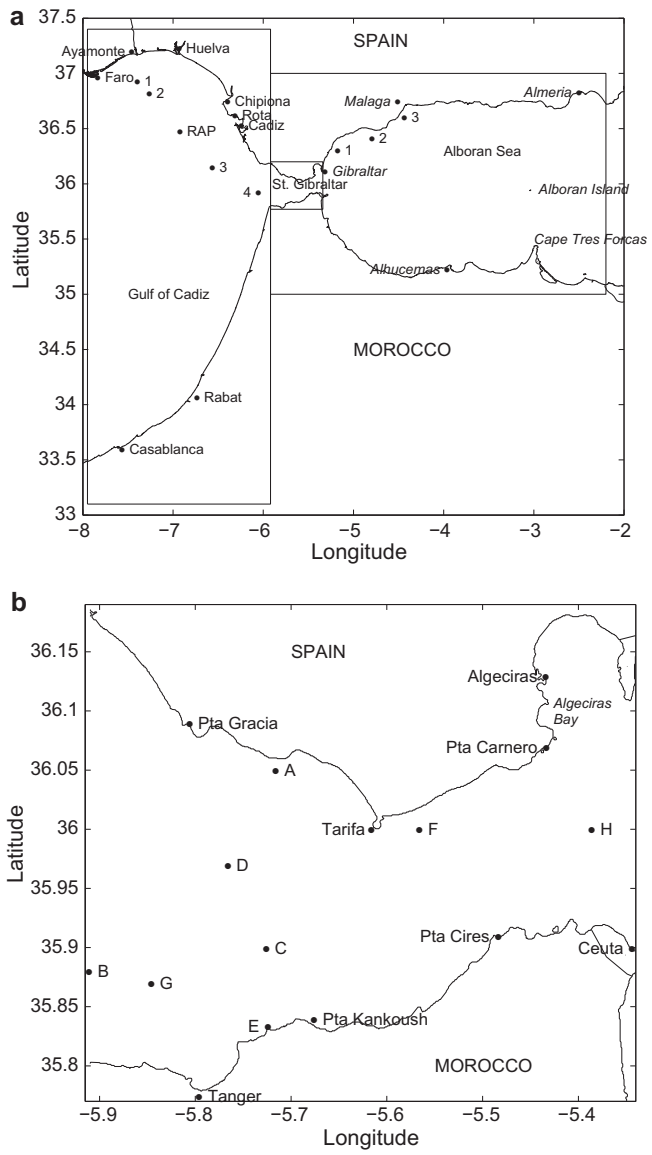

Fig. 1. (a) Model domains for the GoC, AS and GS (rectangular boxes). (b) Detailed view of the GS domain. Locations mentioned in the paper are also indicated.

Dispersion is solved using a particle-tracking method. Thus, the spill is simulated by a number of particles, each of them equivalent to a number of units (for instance kg moles or Bq), whose paths are followed in time. Specific processes for each contaminant are included in the model using stochastic techniques (radioactive decay, oil evaporation and biodegradation). A Monte Carlo random-walk method is used to calculate turbulent diffusion. Contaminant concentrations may be obtained at the desired time from the density of particles per water volume unit.

The hydrodynamic models are described in the following section. Next, the particle-tracking dispersion model is presented. Finally, hydrodynamic model results and some application examples of the dispersion models are discussed.

2. Hydrodynamic models

The water current at any position is obtained through the addition of the instantaneous barotropic tidal current plus a residual (mean or long-term) circulation. In the three domains, tides are computed using a 2D-depth-averaged model, which is a reasonable approach (Dyke, 2001; Yanagi, 1999) already used successfully in the Strait of Gibraltar (Periáñez and Pascual-Granged, 2008). Tidal equations are standard and may be seen, for instance, in Periáñez (2005). The solution of these equations provides water currents at each point in the model domain and for each time step. Currents are treated through standard tidal analysis (Pugh, 1987) and tidal constants are stored in files which will be read by the dispersion models. The two main tidal constituents, M_2 and S_2, are considered. Thus, the hydrodynamic equations are solved for each constituent and tidal analysis is also carried out for each constituent separately. Tidal constants allow a very fast calculation of the tidal current at any time and point in the domain.

From an operative point of view, circulation in GS and the AS may be simplified to a two-layer system with water flowing in opposite directions: an upper layer of Atlantic Water flowing to the east, and a more dense bottom layer flowing to the west (Echevarría et al., 2002). This approach has already been used to study water exchanges between the Atlantic and the Mediterranean by means of numerical models (Izquierdo et al., 2001). Consequently, a two-layer model has been adopted to calculate the residual circulation in domains of the AS and GS. Equations may be seen in the above mentioned reference, for instance.

Complex mixing processes between several water masses occur in the GoC (Criado-Aldeanueva et al., 2006), thus a full 3D primitive-equation baroclinic hydrodynamic model is used for this domain. It is based upon the hydrostatic and Bousssinesq approximations on a β plane. The model includes equations for salinity and temperature evolution and water density is calculated from them using a standard state equation. A one-equation turbulence model has been used to calculate the vertical eddy viscosity. Details on the 3D equations may be seen, for instance, in Kowalick and Murty (1993). A summary of the main characteristics of hydrodynamic models may be seen in Table 1. Equations are also summarized in Appendix A.

Residual circulations in the GoC, GS and AS are again stored in files which are appropriately read by the dispersion codes. It must be pointed out that the three grids are running independently, without any dynamic interaction between them.

3. Particle-tracking dispersion model

Essentially, a pollutant discharge is simulated by a number of discrete, passive, particles, each one equivalent to a number of units. The three-dimensional path followed by each particle is computed, turbulent diffusion being modelled as a three-dimensional random walk process. The density of particles per water volume unit is finally computed to obtain contaminant concentrations over the domain at the desired time and depth. Both instantaneous and continuous releases of particles can be simulated. Specific processes for different pollutants are included as commented below.

Advection is computed solving the following equation for each particle:

$$\frac{d\mathbf{r}}{dt} = \mathbf{q} \tag{1}$$

where $\mathbf{r}$ is the position vector of the particle and $\mathbf{q}$ is the current vector (due to wind, tide and residual circulation) at the particle position and depth, solved in components u and v.

The maximum size of the horizontal step given by the particle due to turbulence, D_h, is:

$$D_h = \sqrt{12 K_h \Delta t} \tag{2}$$

in the direction $\theta = 2\pi RAN$, where RAN is a random number between 0 and 1. This equation gives the maximum size of the step. In practice, it is multiplied by RAN to obtain the real size at a given

Table 1
Summary of hydrodynamic model characteristics.

	2D models	Two-layer models	3D model
Domain	GoC, AS, GS	AS, GS	GoC
Objective	Tides	Mean circulation	Mean circulation
Spatial resolution	2 min[a] (AS, GoC)	2 min[a] (AS)	2 min[a]
	1 km (GS)	1 km (GS)	
Features	Barotropic depth-averaged M_2, S_2 constituents tidal analysis	2 water layers with constant density	Hydrostatic, Boussinesq baroclinic equations for T and S 1-equation turbulence model
Forcing	Tide amplitude and phase along open boundaries	Water exchanges through Gibraltar Strait	Water exchanges through Gibraltar Strait and T, S from climatology
Forcing data source	Schwiderski (1980a,b) Tsimplis et al. (1995)	Preller (1986)	Preller (1986) WOA05 climatology[b]
Additional boundary condition where required	Radiation[c]	Radiation[c]	Radiation[c]

[a] In both longitude and latitude.
[b] World Ocean Atlas 2005, National Ocean and Atmosphere Administration, available on-line. Seasonal values have been used.
[c] See Mellor (2004).

time and for a given particle. Similarly, the maximum size of the vertical step is:

$$D_v = \sqrt{2K_v\Delta t} \tag{3}$$

given either towards the sea surface or the sea bottom. K_h and K_v are the horizontal and vertical diffusion coefficients, respectively, and Δt is time step.

The effect of wind is included as usual in rapid-response particle-tracking models. Thus, it is assumed that the water surface moves in the direction of wind at a speed equal to 3% of the wind speed 10 m above the sea surface. This current decreases logarithmically to zero at a depth usually taken as 20 m. Changing wind fields may be specified as in Periáñez and Pascual-Granged (2008). It may be noted that wind is not included in the hydrodynamic calculations, but only in dispersion. This is the standard approach in rapid-response models, which require current fields computed in advance so that computation time is not drastically increased.

Radioactive decay, in order to simulate radioactive spills, is described using a stochastic method (Periáñez, 2005). Some specific processes for oil have to be included. In addition to advection and three-dimensional diffusion, droplets have a size distribution so that larger ones tend to remain in the water surface and move in the direction of wind. Smaller droplets mix downwards because of turbulence and shear diffusion results in a patch elongated in the current direction. The model also includes the effects of surface evaporation of oil and decomposition within the water column (for instance because of biodegradation). These processes are also simulated using a stochastic method (details may be seen in Periáñez and Pascual-Granged, 2008) through the specification of e-folding times. If during a computation an oil droplet reaches the coastline, it is considered *beached*. Thus, the droplet stays in the coast without moving any more. Equations describing all these processes are presented in Appendix B. This formulation has been carefully tested comparing model results with observations during the Arabian Gulf oil spill. Additionally, the particle-tracking method has been compared, in the case of radioactive spills, with a finite difference formulation (Periáñez and Elliott, 2002). Very good agreement between both techniques was obtained.

Values for the diffusion coefficients have to be provided. The horizontal diffusion coefficient depends on the horizontal grid spacing. Following Dick and Schonfeld (1996):

$$K_h = 0.2055 \times 10^{-3}\Delta x^{1.15} \tag{4}$$

The present grid resolutions give $K_h = 0.58$ m^2/s for GS and $K_h = 2.0$ m^2/s for GoC and AS domains. In the case of the vertical diffusion coefficient, a typical value of 0.001 m^2/s is used (Elliott et al., 2001; Schonfeld, 1995; Dick and Schonfeld, 1996; Elliott, 1999).

Date and time of the discharge (and duration in the case of continuous releases) must be specified since the fate of the release will depend on the tidal state when it took place. Thus, the appropriate phase of each tidal constituent at $t = 0$ must be specified. The values used correspond to the origin of time being January 1, 2003 at 0:15 h Greenwich time.

Input data required by the dispersion model is summarized in Table 2. The meaning of the residual current modulator is explained below (see Section 4.2).

The model output consists of twelve snapshots at constant intervals during the simulation, to show the evolution of the radionuclide patch over time. These snapshots can be drawn in a 3D form, or as projections on the *xy*, *xz* and *yz* planes. Pollutant concentration maps at any depth are obtained from the density of particles per water volume unit.

It should be commented that the 3D particle-tracking dispersion model is the same in the three domains. The only difference is due to the residual currents provided by the hydrodynamic models. Thus, these currents already have a 3D structure in the GoC, while depth averaged currents for each water layer are given for AS and GS. In these cases, the 3D current required by the particle-tracking model is constructed from the mean current in each layer using a standard current profile (Riddle, 1998), usually applied in this kind of models. The same method is used to construct a vertical profile for the tidal current calculated by the depth-averaged barotropic tidal model in each domain.

4. Results and discussion

4.1. Hydrodynamics

4.1.1. Tides

Results of the 2D barotropic tidal model in each domain have been validated through comparisons of calculated tidal amplitudes and phases with measurements in the sea. Such comparisons are presented in Tables 3–5 for the GoC, GS and AS, respectively.

It may be seen that, generally, there is a good agreement between both set of data. The amplitude of the tide is about 1 m over all the GoC, decreasing near the Strait of Gibraltar. Associated currents are weak, with amplitudes below 0.10 m/s over most of the GoC. Indeed at the RAP (Red de Aguas Profundas, Spanish Institute of Oceanography) buoy position (see Fig. 1a), the M_2 barotropic tidal current is less than 0.03 m/s (García-Lafuente et al., 2006). The computed current at this position is 0.034 m/s. The current amplitude increases as approaching the Strait entrance, where currents about 0.8 m/s are produced. A similar behaviour is observed for the S_2 tide.

In GS there is an amplitude reduction in a factor 2, approximately, along the Strait in both tides, and essentially constant amplitudes across the Strait. A comparison between computed and barotropic current amplitudes and phases deduced from measurements (Mañanes et al., 1998) in the Strait can be seen in

Table 2
Information required by the model to be introduced by user.

Release point coordinates
Select instantaneous/continuous release option
Wind data file
Release date (day, month, year)
Release time, UTC, (h, min)
Residual current modulator
Simulation time (days)
Magnitude of the release in the corresponding units[a]
Contaminant decay constant (radioactive)
Oil spill additional information
Oil density
Droplet minimum and maximum sizes
e-Folding times (evaporation and decomposition)

[a] In case of a continuous release, release rate is assumed to be constant along the duration of the accident.

Table 3
Established, index *obs*, (NOAA, 1982) and computed, index *comp*, amplitudes (A, cm) and phases (g, deg) of tidal elevations at several locations indicated in Fig. 1 (GoC domain).

Station	M_2				S_2			
	A_{obs}	g_{obs}	A_{comp}	g_{comp}	A_{obs}	g_{obs}	A_{comp}	g_{comp}
Faro	92	94	99	68	32	125	36	91
Chipiona	102	54	104	62	41	82	38	85
Rota	105	52	103	62	37	78	38	85
Cadiz	100	87	99	61	37	110	36	83
Ayamonte	100	59	101	65	32	88	36	89
Huelva	102	56	105	65	38	82	38	88
Casablanca	99	56	92	53	35	81	36	77
Rabat	88	59	98	57	35	83	36	78

Table 4
Observed (Candela et al., 1990) and computed amplitudes (A, cm) and phases (g, deg) of tidal elevations at some locations indicated in Fig. 1b (GS domain).

Station	M_2				S_2			
	A_{obs}	g_{obs}	A_{comp}	g_{comp}	A_{obs}	g_{obs}	A_{comp}	g_{comp}
Pta Gracia	64.9	49	71.9	59	22.3	74	24.9	82
D	60.1	52	57.5	53	22.5	74	21.4	79
C	54.0	62	54.1	54	21.1	83	20.0	82
A	52.3	48	57.5	54	18.5	73	20.9	79
E	57.1	67	59.8	60	20.6	92	21.4	87
B	78.5	56	78.5	64	29.0	82	27.0	89
Pta Kankoush	51.8	69	51.3	54	20.1	90	19.1	83
Tarifa	41.5	57	42.9	46	14.2	85	16.6	73
F	44.4	48	39.8	45	16.1	74	15.4	72
Pta Cires	36.4	47	37.8	52	14.1	74	14.0	79
Algeciras	31.0	48	29.1	47	11.1	74	11.0	72
Pta Carnero	31.1	48	29.1	46	11.5	71	11.0	71
Ceuta	29.7	50	29.6	52	11.4	76	10.9	74

Table 5
Observed (Tsimplis et al., 1995; Manzella and Elliott, 1991) and computed amplitudes (A, cm) and phases (g, deg) of tidal elevations at several locations indicated in Fig. 1 (AS domain).

Station	M_2				S_2			
	A_{obs}	g_{obs}	A_{comp}	g_{comp}	A_{obs}	g_{obs}	A_{comp}	g_{comp}
Tarifa	42	57	41	45	14	85	16	79
Ceuta	30	50	32	52	11	76	12	86
Málaga	17	59	18	42	7	72	8	77
Alhucemas	18	58	18	56	7	80	7	89
Almería	9	51	9	49	4	78	4	77
Gibraltar	30	46	29	41	11	72	12	77

Table 6. The agreement in currents is not as good as in the case of tidal elevations, specially for the M_2 tide. However, the difficulty in appropriately defining the barotropic current has already been commented by Tejedor et al. (1999) when they compared barotropic currents predicted by their model with those derived from observations in the Strait.

There is a further, although slower, tide amplitude reduction in AS, reaching only some 0.10 m at the eastern boundary for the M_2 tide. Corange lines are, like in GS, oriented in a south-north direction. A comparison of computed M_2 current ellipse parameters with those deduced from measurements (García-Lafuente and Cayo-Lucana, 1994) is presented in Table 7. In general, there is a good agreement between both set of data.

4.1.2. Mean flows

The residual surface circulation in the northern GoC is characterized by a current directed to the SE (Criado-Aldeanueva et al., 2006) along the Spanish coast. This circulation is a rather constant pattern along the year. Part of the flow enters the Strait of Gibraltar and part is deflected to the south. The residual circulation computed with the baroclinic model at the sea surface is presented in Fig. 2. The current is effectively directed to the SE over the Spanish continental shelf and part of this flow enters the Strait of Gibraltar. Maximum currents are of the order of 0.3 m/s, in agreement with García-Lafuente et al. (2006). The anticyclonic eddy at the east of Faro (see Fig. 1a) has been described by Machín et al. (2006). Also, the cyclonic eddy in front of the Strait of Gibraltar appears clearly in the model of Peliz et al. (2007), who attributed it to the strong convergence occurring in this area.

Below the surface, the Mediterranean waters flow into the Atlantic and mainly direct to the NW (Serra et al., 2005). As an example, the computed circulation 590 m below the surface is presented in Fig. 3. Only the northern part of the GoC is shown to appreciate details more clearly. These currents are in agreement with the geostrophic velocities below 400 m, referenced to 300 m, provided by Criado-Aldeanueva et al. (2006) and with the calculations by Peliz et al. (2007). Water velocity is higher close to the Strait and then slows to about 0.1 m/s, in agreement with Ambar and Howe (1979).

The calculated geostrophic flows for the upper and lower layers in AS, for the mean water exchanges through the Strait of Gibraltar, are presented in Fig. 4. In the upper layer, the jet of Atlantic water entering through the Strait of Gibraltar flows towards the east along the Spanish coast and partially curves to the south before reaching Alborán Island. Part of this flow continues to the east between Cape Tres Forcas and Alborán Island and the remaining rotates towards the west. A gyre of anticyclonic circulation is thus

Table 6
Observed (Mañanes et al., 1998) and computed amplitudes (q, m/s) and phases (g, deg) of M_2 and S_2 barotropic tidal velocities at three locations in Fig. 1b (GS domain).

Station	M_2				S_2			
	q_{obs}	g_{obs}	q_{comp}	g_{comp}	q_{obs}	g_{obs}	q_{comp}	g_{comp}
C	0.91	147	0.94	126	0.31	171	0.37	177
H	0.25	160	0.31	115	0.12	178	0.13	154
G	0.65	157	0.62	129	0.23	182	0.25	172

Table 7
Computed and measured (García-Lafuente and Cayo-Lucana, 1994) current ellipse parameters for the M_2 tide at points indicated with numbers in Fig. 1a (AS domain). M and m are the magnitudes of the major and minor semiaxes, respectively, and dir is the direction of the major semiaxis measured anticlockwise from east.

Station	Measured values			Computed values		
	M (m/s)	dir (deg)	m (m/s)	M (m/s)	dir (deg)	m (m/s)
1	0.09	54	0.02	0.14	57	0.01
2	0.06	4	0.005	0.05	7	0.001
3	0.04	45	0.02	0.02	67	0.01

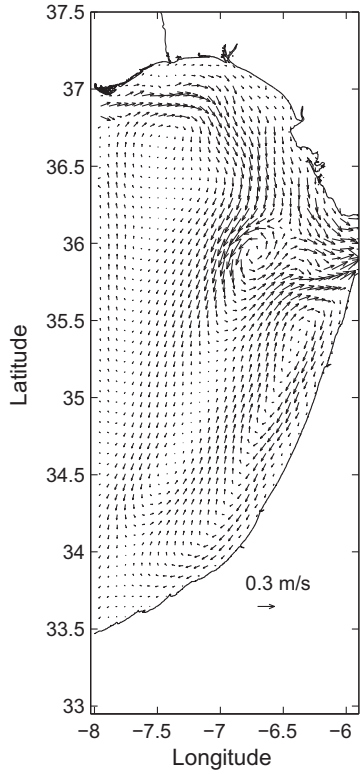

Fig. 2. Computed surface residual currents in GoC. Only one of each 4 vectors is drawn.

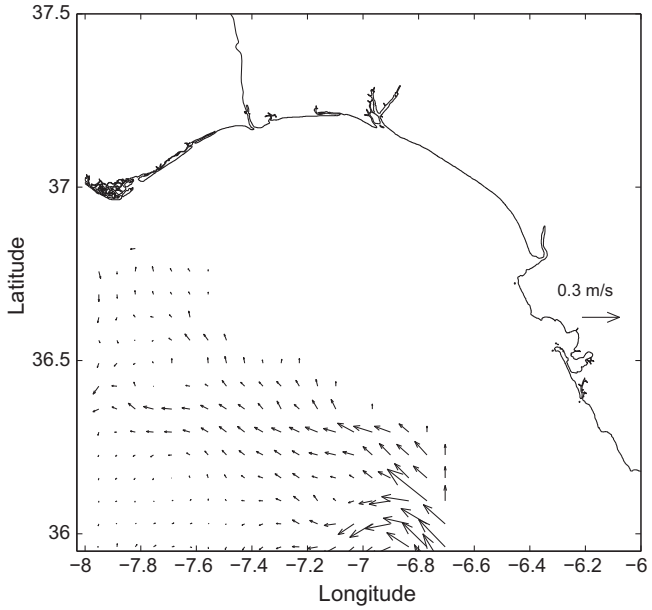

Fig. 3. Computed residual currents 590 m below the surface in the northern GoC. Only one of each 4 vectors is drawn.

completed. It is known as the Western Alborán Gyre, which is an almost constant feature of AS surface circulation (Werner et al., 1988). Surface water velocity in the Strait reaches 0.53 m/s, in agreement with the current speeds of the order of 0.6 m/s reported from measurements (Perkins et al., 1990) and models (Sannino et al., 2004). In the jet, along the Spanish coast, maximum surface velocities are of the order of 0.4 m/s. Measurements of Perkins et al. (1990) in this area range between 0.1 and 0.53 m/s and the model of Werner et al. (1988) produces maximum currents in the north of the gyre of 0.25 m/s. Vargas-Yáñez et al. (2002) have measured eastward geostrophic velocities in the passage between Cape tres Forcas and Alborán Island (see Fig. 1a). They are 11 ± 5, 5 ± 3 and 1 ± 3 cm/s at depths of 74, 117 and 178 m, respectively (all depths correspond to the surface layer). Computed current at the same point for the surface layer is 3.8 cm/s.

A westward circulation is obtained for the bottom layer. In the western Strait of Gibraltar computed velocities are of the order of 0.20 m/s, in good agreement with the 0.15 m/s obtained by Béranguer et al. (2005). Maximum outflow current calculated in the Strait is 0.36 m/s; Sannino et al. (2002) obtained a figure of 0.35 m/s. In the Alborán Sea, water velocities are reduced to some 0.1 m/s in the southern area and less in the northern part of the basin. This circulation pattern for the deep layer is in good agreement with the earlier calculations of Preller (1986), that also show that most of the deep water flows along the south coast with speed below 0.15 m/s, and with measurements in Gascard and Richez (1985), who give velocities in the southern shelf, near the Strait, of 0.1 m/s. Bryden and Stommel (1982) have also found, from CTD transects, that the westward deep flow occurs along the Moroccan continental slope. These authors have measured a mean (using a 341-day record) outflow velocity of 4.6 ± 0.6 cm/s in a point located at about -4.6° longitude and over the 500 m isobath in the Moroccan continental slope. They do not give the exact position of the current meter mooring, but the model predicts (for such longitude and a depth of 535 m) a westward current equal to 3.6 cm/s.

Finally, the mean circulation in the two layers of GS may be seen in Fig. 5. Currents are directed along GS axis. The magnitude of the mean surface currents increases as going to the east. The u component (approximately along-strait) of the mean surface current magnitude along the axis of the Strait is presented in Fig. 6 together with the earlier calculations of Sannino et al. (2004).

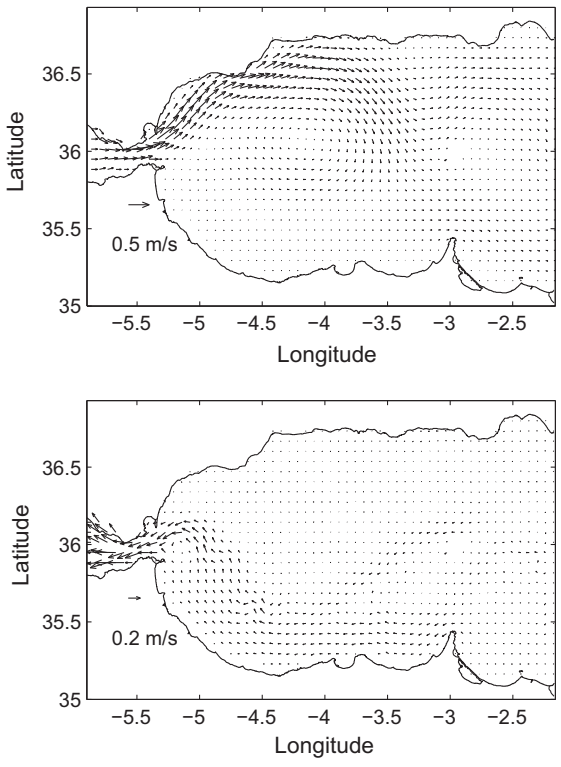

Fig. 4. Computed residual currents in the upper (up) and lower (down) water layers of the AS. Only one of each four computed vectors is shown for clarity.

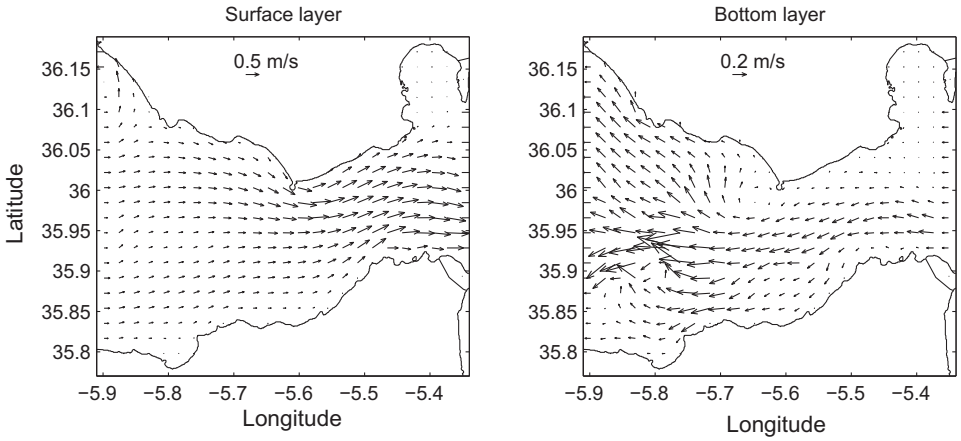

Fig. 5. Computed residual currents in the upper and lower water layers of the GS. Only one of each four computed vectors is shown for clarity.

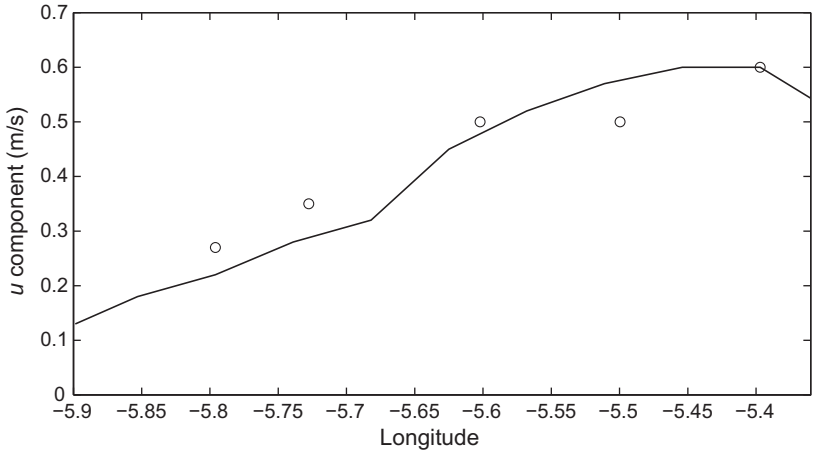

Fig. 6. Computed *u* component of the mean current along the axis of GS (line). Points correspond to results of Sannino et al. (2004).

Perkins et al. (1990) have also measured currents of the order of 0.6 m/s in surface water of GS. It may be seen that both models give very similar residual currents along the Strait. In the deep layer currents are, obviously, directed to the Atlantic Ocean. Calculated maximum outflow currents are obtained over Camarinal Sill (at approximately the center of GS and at -5.75° latitude), resulting 0.67 m/s. Measurements in this area have given 0.60 m/s (Bryden et al., 1994) and 0.65 m/s (Tsimplis and Bryden, 2000). Computed maximum outflow currents are higher than with the AS two-layer model (see above) and are also closer to actual values. This must be attributed to the higher spatial resolution in the GS domain.

Thus, it seems that hydrodynamic models are providing a realistic view of tidal and mean circulations in southern Spain coastal waters, and particle-tracking dispersion models will use these computed currents to assess pollutant transport.

4.2. Dispersion

It must be commented that the mean currents in the domains, which are obtained for the mean water exchanges through GS, are also affected by other factors as for instance atmospheric pressure differences between the Atlantic and the western Mediterranean, and thus presents some variability. Consequently, a factor that acts as a modulator of the residual current amplitude has been introduced. If 1 is used, the residual current for the mean water exchanges through GS is used in the calculations. These mean currents may be amplified or reduced by specifying values for the modulator larger or smaller than 1, respectively.

It is worth commenting that it is difficult to provide a value for this modulator: let us imagine that an accident occurs just now. How do we run the model? In other words: Which is the water inflow through the Strait just now? Presently it is not possible to have an answer. Thus, it is recommended to carry out calculations under the most probable conditions in a first guess (using the mean current, with a modulator equal to 1). Additional simulations may then be carried out using other current modulators to increase and reduce water velocities. This method will, at least, allow to estimate if there is any chance that a given sensible point (a coastal town for instance) is affected by contamination in a given time. Given the short running times of the models (a few seconds per day of simulation on a Pentium 4 PC in the case of an instantaneous release), this is not a problem. This procedure has already been suggested for a spill model recently developed for the Alborán Sea (Periáñez, 2007) as well as by Sotillo et al. (2008). In all examples presented below, the modulator is set to 1. Also, in the case of a real accident a rapid-response system should give information on the expected situation a few hours-days after the spill. The three grids run independently, as was commented before. Thus, the grid used to make calculations will depend on the location of the spill. If it occurs in the surface of the Strait of Gibraltar, for instance, the GS grid may be used to see the detailed movement of the patch inside the Strait and, simultaneously, the AS grid provides information on

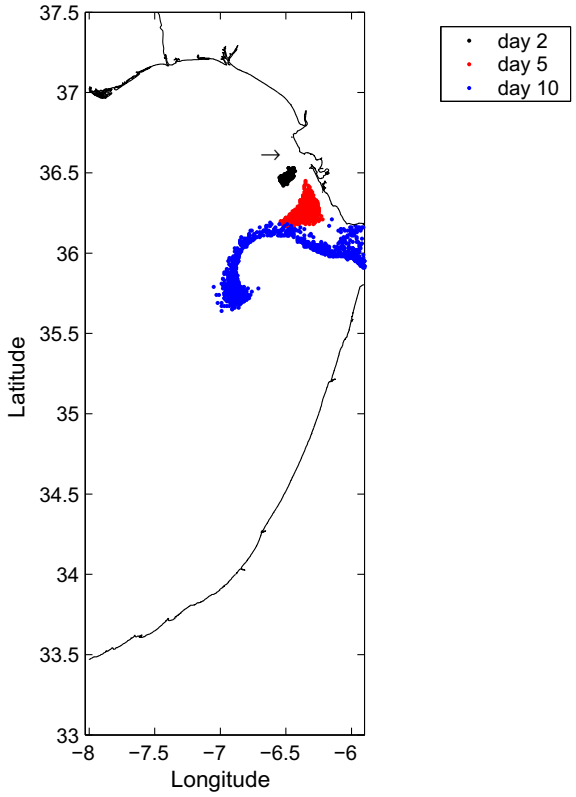

Fig. 7. Position of particles 2, 5 and 10 days after an instantaneous surface chemical spill occurring at the arrow position.

how it enters the Alborán Sea, as a result of the mean circulation, after a few days.

Ideally, results from the dispersion models should be compared with observations after real accidents in the different domains. However, there are no data to carry out this work. Thus, we could only simulate some hypothetical accidents simply to show that results are logical and consistent. Nevertheless, if must be mentioned that calculated currents in the GoC and AS have been successfully used to simulate, respectively, heavy metal and fallout radionuclide dispersion in these domains (Periáñez, 2008, 2009). This is providing some additional confidence in hydrodynamic model results and, consequently, also in results of the Lagrangian dispersion model.

The first numerical experiment consisted of a chemical spill occurring in front of the Bay of Cádiz (GoC), coordinates $(-6.54^{\circ}, 36.62^{\circ})$. The spill was an instantaneous release at the surface on January 1, 2008 at 0:00 h (this date and time were taken just as an example) and with no wind. Snapshots showing the position of particles 2, 5 and 10 days after the accident may be seen in Fig. 7. These snapshots are projections of the three-dimensional particle positions on the *xy* plane. The contamination patch is transported towards the Strait of Gibraltar by the residual current, although some is directed to the west by the gyre existing in front of the Strait (Fig. 2). A significant fraction of the spill has entered the Mediterranean through the Strait after 12 days.

A second experiment consisted of a release from a sunken nuclear submarine in front of Gibraltar (coordinates $-5.27^{\circ}, 36.10^{\circ}$). The release is assumed to be instantaneous (total amount 1.0×10^{12} Bq) and to occur just over the seabed (water depth 500 m at this point). The accidental release takes place at the same date and time as before and again no wind is considered. Some examples of results are presented in Fig. 8. Two maps showing radionuclide concentrations 12 days after the accident in the sur-

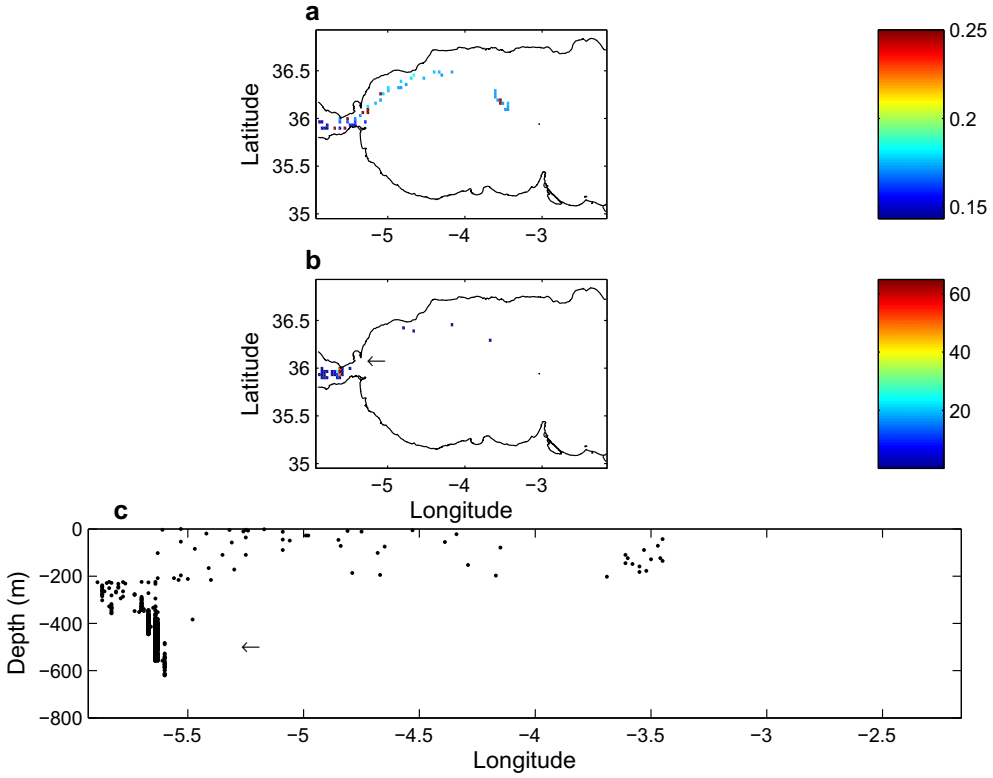

Fig. 8. Radionuclide concentrations (Bq/m^3) in the upper (a) and lower (b) water layers of the AS 12 days after the release (see text). (c) Projection of particle positions on the *xz* plane. The position of the release is indicated by the arrow in panels b and c.

face and bottom water layers are presented in Fig. 8a and b, respectively. In the bottom water layer the current is directed to the west and, consequently, most of the radionuclides move in this direction. Nevertheless, some of them cross the pycnocline (the interface separating both water layers) and reach the surface water layer, which moves to the east (see Fig. 4). Thus, a fraction of the release is transported to the east along the Spanish coast. Later this radionuclide patch is deflected to the south by the Western Alboran Gyre. A projection of particle positions 12 days after the accident on the *xz* plane is presented in Fig. 8c. The pycnocline depth in the AS is in the range of approximately 170 to 220 m. It acts as a natural barrier for mixing and, indeed, only a small fraction of the release crosses it, as it may be seen comparing the color scales in Fig. 8. Water depths in the Strait of Gibraltar decrease very fast from about -5.5° towards the west. Most of the patch is trapped in this abrupt slope (see Fig. 8c). Also, it is in this region of abrupt topography where mixing through the pycnocline mainly occurs. Experiments in other parts of the AS, concerning releases at the same depth, have not shown any significant mixing through the interface.

Finally, an oil spill has been simulated in GS. This example also provides an illustration of a continuous release. Date and time of the accident is again the same as before. This time, however, a 5 m/s east wind, which is typical in this area, has been considered. An oil spill is supposed to occur at the arrow position (coordinates $-5.74^{\circ}, 36.02^{\circ}$), on the sea surface, during 48 h. Oil is heavy fuel with density 1010 kg/m^3, which is the same released during the Prestige crisis (Carracedo et al., 2006). Droplet size is in the range 60—600 μm and e-folding times are 25 and 250 h for evaporation and decomposition, respectively. These are typical values (Proctor et al., 1994; Korotenko et al., 2004). Results of the experiment may be seen in Fig. 9, where particle positions at different times are shown. It may be seen that a plume, typical of continuous releases, is formed. Oil moves to the east because of the surface residual currents in GS, but the effect of tidal oscillations may be appreciated in the curved shapes adopted by the plume. It can also be seen that the Spanish coast starts to be contaminated by oil some 24 h after the beginning of the accident. After 48 h, the contaminated coast extends almost from Tarifa to Pta Carnero (see Fig. 1b). Winds from the east tend to enhance transverse mixing in the Strait, as they oppose the residual circulation. On the contrary, during calm or west wind episodes contaminants are more rapidly flushed off the Strait, as other numerical experiments have pointed out.

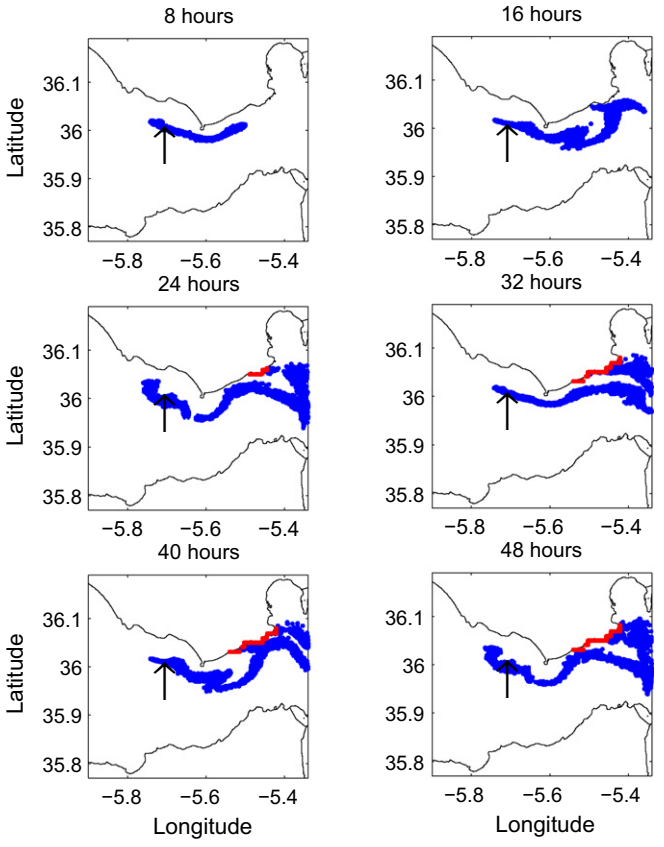

Fig. 9. Position of beached oil particles (red) and oil particles in water (blue) at different times after the beginning of a continuous surface oil spill in GS. The spill occurs at the arrow position. (For interpretation of the references to color in this figure legend, the reader is referred to the web version of this article.)

5. Conclusions

Rapid-response particle-tracking dispersion models, which are appropriate tools to support the decision-making process after an emergency situation, have been developed for southern Spain coastal waters. Three domains covering Atlantic, Mediterranean waters and the Strait of Gibraltar (at higher spatial resolution) have been included. Dispersion models may be applied to chemical, radioactive and oil spills.

Water circulation is obtained from appropriate hydrodynamic models, which are run off-line (in advance) and validated through comparisons with observations in the regions. Tides are calculated using a 2D barotropic model in the three domains. Models used to obtain the residual circulation depend on the physical oceanography of each region. Thus, two-layer models are applied to Gibraltar Strait and Alborán Sea and a 3D baroclinic model is used in the Gulf of Cádiz. Tides (actually tidal constants obtained after a standard tidal analysis procedure) and residual currents are stored in files which are later read by the dispersion models. Specific processes for oil and radioactive spills are included, being simulated using stochastic methods.

Although results of these dispersion models could not be compared with observations, several examples concerning hypothetical accidents in each domain have been presented and discussed, indicating that results are consistent and meaningful. These numerical experiments, moreover, are useful to improve our knowledge about processes occurring in the environment. For instance, it has been found that mixing of contaminants through the pycnocline in the Alborán Sea essentially occurs in the area of abrupt topography change of the Strait of Gibraltar.

Acknowledgements

The authors are indebted to the Agencia Española de Cooperación Internacional for partially funding this work. R. Periáñez is also indebted to the Spanish Ministerio de Educación y Ciencia for a fellowship to stay during three months at the University of Wales, Bangor, where part of this work was carried out.

Appendix A. Hydrodynamic models

A.1. 2D barotropic model

The 2D-depth-averaged model used to compute tides is based on the following equations:

$$\frac{\partial \zeta}{\partial t} + \frac{\partial}{\partial x}(Hu) + \frac{\partial}{\partial y}(Hv) = 0 \tag{5}$$

$$\frac{\partial u}{\partial t} + u\frac{\partial u}{\partial x} + v\frac{\partial u}{\partial y} + g\frac{\partial \zeta}{\partial x} - \Omega v + \frac{\tau_u}{\rho_w H} = A\left(\frac{\partial^2 u}{\partial x^2} + \frac{\partial^2 u}{\partial y^2}\right) \tag{6}$$

$$\frac{\partial v}{\partial t}+u\frac{\partial v}{\partial x}+v\frac{\partial v}{\partial y}+g\frac{\partial \zeta}{\partial y}+\Omega u+\frac{\tau_v}{\rho_w H}=A\left(\frac{\partial^2 v}{\partial x^2}+\frac{\partial^2 v}{\partial y^2}\right) \tag{7}$$

where u and v are the depth averaged water velocities along the x and y axis, h is the depth of water below the mean sea level, ζ is the displacement of the water surface above the mean sea level measured upwards, $H=h+\zeta$ is the total water depth, Ω is the Coriolis parameter ($\Omega=2w\sin\beta$, where w is the Earth rotational angular velocity and β is latitude), g is acceleration due to gravity, ρ_w is water density and A is the horizontal eddy viscosity. τ_u and τ_v are friction stresses that have been written in terms of a quadratic law:

$$\begin{aligned}\tau_u&=k\rho_w u\sqrt{u^2+v^2}\\ \tau_v&=k\rho_w v\sqrt{u^2+v^2}\end{aligned} \tag{8}$$

where k is the bed friction coefficient.

A.2. 3D baroclinic model

The full 3D hydrodynamic equations including the terms corresponding to density gradients are written in the hydrostatic and Boussinesq approximations as:

$$\frac{\partial \zeta}{\partial t}+\frac{\partial}{\partial x}\left[(h+\zeta)\int_{-h}^{\zeta}u\mathrm{d}z\right]+\frac{\partial}{\partial y}\left[(h+\zeta)\int_{-h}^{\zeta}v\mathrm{d}z\right]=0 \tag{9}$$

$$\begin{aligned}&\frac{\partial u}{\partial t}+u\frac{\partial u}{\partial x}+v\frac{\partial u}{\partial y}-\Omega v+g\frac{\partial \zeta}{\partial x}+\frac{g}{\rho_0}\int_z^{\zeta}\frac{\partial \rho_w}{\partial x}\mathrm{d}z\\ &\quad=\frac{\partial}{\partial z}\left(K\frac{\partial u}{\partial z}\right)+A\left(\frac{\partial^2 u}{\partial x^2}+\frac{\partial^2 u}{\partial y^2}\right)\end{aligned} \tag{10}$$

$$\begin{aligned}&\frac{\partial v}{\partial t}+u\frac{\partial v}{\partial x}+v\frac{\partial v}{\partial y}+\Omega u+g\frac{\partial \zeta}{\partial y}+\frac{g}{\rho_0}\int_z^{\zeta}\frac{\partial \rho_w}{\partial y}\mathrm{d}z\\ &\quad=\frac{\partial}{\partial z}\left(K\frac{\partial v}{\partial z}\right)+A\left(\frac{\partial^2 v}{\partial x^2}+\frac{\partial^2 v}{\partial y^2}\right)\end{aligned} \tag{11}$$

where ρ_w is water density, ρ_0 is a reference density, and K and A are the vertical and horizontal eddy viscosities, respectively.

The vertical component of the water velocity, w, is obtained from the continuity equation:

$$\frac{\partial u}{\partial x}+\frac{\partial v}{\partial y}+\frac{\partial w}{\partial z}=0 \tag{12}$$

The water density is derived from a equation of state relating density to salinity and temperature:

$$\rho_w=\rho_0[1-\alpha(T-T_0)+\beta(S-S_0)] \tag{13}$$

where S is salinity, T is temperature, $\alpha=2.41\times10^{-4}$ and $\beta=7.45\times10^{-4}$. The reference salinity is taken as $\rho_0=999.7$ kg/m^3 at $S_0=0$ and $T_0=10$ °C.

Water salinity is determined from an advection-diffusion equation:

$$\frac{\partial S}{\partial t}+u\frac{\partial S}{\partial x}+v\frac{\partial S}{\partial y}+w\frac{\partial S}{\partial z}=A\left(\frac{\partial^2 S}{\partial x^2}+\frac{\partial^2 S}{\partial y^2}\right)+\frac{\partial}{\partial z}\left(K\frac{\partial S}{\partial z}\right) \tag{14}$$

and a similar equation is used for temperature:

$$\frac{\partial T}{\partial t}+u\frac{\partial T}{\partial x}+v\frac{\partial T}{\partial y}+w\frac{\partial T}{\partial z}=A\left(\frac{\partial^2 T}{\partial x^2}+\frac{\partial^2 T}{\partial y^2}\right)+\frac{\partial}{\partial z}\left(K\frac{\partial T}{\partial z}\right) \tag{15}$$

Vertical eddy viscosity is determined from a 1-equation turbulence model. The equation for the turbulent kinetic energy E is:

$$\frac{\partial E}{\partial t}=K\left\{\left(\frac{\partial u}{\partial z}\right)^2+\left(\frac{\partial v}{\partial z}\right)^2\right\}+\beta_0\frac{\partial}{\partial z}\left(K\frac{\partial E}{\partial z}\right)-\varepsilon+\frac{g}{\rho_0}K\frac{\partial \rho}{\partial z} \tag{16}$$

The first term in the right side of the equation represents generation of turbulence by the vertical shear, the second term is diffusion of turbulence and the last term is loss of turbulence by bouyancy (conversion of kinetic energy into potential energy). ε represents dissipation of turbulence, that is written as:

$$\varepsilon=C_1E^{3/2}\ell \tag{17}$$

where ℓ is a mixing length and C_1 a numeric coefficient. The vertical viscosity is finally written as a function of energy as:

$$K=C_0\ell E^{1/2}+\lambda_t \tag{18}$$

where C_0 is a numeric coefficient and λ_t is a background value of viscosity, that is the minimum possible value that it may have. The values of the numeric constants appearing above are: $\beta_0=0.73$, $C_0=C^{1/4}$, $C_1=C_0^3$ and $C=0.046$. The background viscosity is fixed as $\lambda_t=10^{-4}$ m^2/s.

The mixing length is derived from an algebraic expression:

$$\ell=\frac{1}{1/\ell_1+1/\ell_2} \tag{19}$$

with

$$\ell_1=\kappa(z+z_0+h)e^{\beta_1\frac{z+h}{h}} \tag{20}$$

$$\ell_2=\kappa(z_s-z) \tag{21}$$

where $\kappa=0.4$ is the von Karman's constant, $\beta_1=-2.0$ and z_s and z_0 are the roughness lengths of the sea surface and bottom, respectively.

A.3. Two-layer model

Two water layers with different densities are flowing in opposite directions in the Alborán Sea. The equations describing this flow are the following (in the vector formulation of Izquierdo et al., 2001):

$$\begin{aligned}&\frac{\partial(H_1\vec{u_1})}{\partial t}+\nabla(H_1\vec{u_1}\cdot\vec{u_1})+\Omega\vec{k}\times H_1\vec{u_1}+gH_1\nabla\zeta_1\\ &\quad=-\vec{\tau_1}/\rho_1+AH_1\nabla^2\vec{u_1}\end{aligned} \tag{22}$$

$$\frac{\partial H_1}{\partial t}+\nabla\cdot H_1\vec{u_1}=0 \tag{23}$$

$$\begin{aligned}&\frac{\partial(H_2\vec{u_2})}{\partial t}+\nabla(H_2\vec{u_2}\cdot\vec{u_2})+\Omega\vec{k}\times H_2\vec{u_2}+g\frac{\rho_1}{\rho_2}H_2\nabla\zeta_1+g'H_2\nabla\zeta_2\\ &\quad=(\vec{\tau_1}-\vec{\tau_2})/\rho_2+AH_2\nabla^2\vec{u_2}\end{aligned} \tag{24}$$

$$\frac{\partial H_2}{\partial t}+\nabla\cdot H_2\vec{u_2}=0 \tag{25}$$

with indexes 1 and 2 for the upper and lower layers, respectively. In these equations H_i is the thickness of the water layer, ρ_i is water density in each layer, A is a horizontal friction coefficient and g' is the reduced gravity:

$$g'=g\frac{\rho_2-\rho_1}{\rho_2} \tag{26}$$

ζ_1 is the elevation of the sea surface with respect to the mean level and ζ_2 is the depth of the interface between layers. Finally $\vec{\tau_1}$ and $\vec{\tau_2}$ are friction stresses between water layers and between the lower layer and the seabed, respectively. They are formulated in terms of a quadratic law as usual:

$$\vec{\tau}_1 = c_1\rho_1|\vec{u_1} - \vec{u_2}|(\vec{u_1} - \vec{u_2})$$
$$\vec{\tau}_2 = c_2\rho_2|\vec{u_2}|\vec{u_2} \quad (27)$$

where c_1 and c_2 are the interfacial and bottom friction coefficients. No significant differences in model results were observed between a f-plane and a β-plane approach, thus the first was used.

Appendix B. Dispersion processes

Radioactive decay can be treated using a stochastic method if it is assumed that the probability p of removal of a particle at each time step is:

$$p = 1 - e^{-\lambda\Delta t} \quad (28)$$

where λ is the radioactive decay constant. In practice, a random number is generated for each particle at each time step. If $RAN \leqslant p$ then the particle is removed from the computation. Obviously, in the case of a stable chemical pollutant $\lambda = 0$.

In the case of oil spills the buoyancy force depends on the density and size of droplets. The vertical velocity, w, can be described as (Proctor et al., 1994; Korotenko et al., 2004):

$$w = \frac{gd^2(1 - \rho_0/\rho_w)}{18\nu} \quad (29)$$

for small droplets with diameter $d \leqslant d_c$ (laminar motion). In this equation ρ_w and ρ_0 are the densities of water and oil, respectively, and ν is the water kinematic viscosity. For large droplets with $d > d_c$ (turbulent motion) the vertical velocity is:

$$w = \left(\frac{8}{3}gd(1 - \rho_0/\rho_w)\right)^{1/2} \quad (30)$$

The critical diameter, d_c, is given by the expression

$$d_c = \frac{9.52\nu^{2/3}}{g^{1/3}(1 - \rho_0/\rho_w)^{1/3}} \quad (31)$$

that is deduced matching the Reynolds numbers at which the transition from laminar to turbulent flow occurs.

The diameter of each oil droplet in the simulation is assigned randomly between a minimum and maximum diameter, $d_{min} - d_{max}$.

The effects of oil evaporation and decomposition are treated in a similar way as radioactive decay using e-folding times (Proctor et al., 1994). Thus, the probability of removal of particle in a time step is given by Eq. (28). The decay constant is related to the e-folding time by $\lambda = 1/T_e$. Different e-folding times are used for evaporation, T_{ev}, and decomposition, T_{de}. Additionally, only particles within a depth $z_{ev} = 0.25$ m below the surface can be evaporated, whereas droplets at any depth can experience decomposition. If during a computation an oil droplet reaches the coastline, it is considered *beached*. Thus, the droplet stays in the coast without moving any more. In the case of a chemical or radioactive spill particles are simply reflected at the coastline. Particles which leave the model domain through an open boundary are removed from the computation.

References

Ambar, I., Howe, M.R., 1979. Observations of the Mediterranean outflow. 2: the deep circulation in the vicinity of the Gulf of Cadiz. Deep Sea Research 26 A, 555–568.

Béranguer, K., Mortier, L., Crépon, M., 2005. Seasonal variability of water transport through the Straits of Gibraltar, Sicily and Corsica, derived from a high-resolution model of the Mediterranean circulation. Progress in Oceanography 66, 341–364.

Bryden, H.L., Candela, J., Kinder, T.H., 1994. Exchange through the Strait of Gibraltar. Progress in Oceanography 33, 201–248.

Bryden, H.L., Stommel, H.M., 1982. Origin of the Mediterranean outflow. Journal of Marine Research 40, 55–71.

Candela, J., Winant, C., Ruiz, A., 1990. Tides in the Strait of Gibraltar. Journal of Geophysical Research 95, 7313–7335.

Carracedo, P., Torres-López, S., Barreiro, M., Montero, P., Balseiro, C.F., Penabad, E., Leitao, P.C., Pérez-Muñuzuri, V., 2006. Improvement of pollutant drift forecast system applied to the Prestige oil spills in Galicia Coast (NW of Spain): development of an operational system. Marine Pollution Bulletin 53, 350–360.

Criado-Aldeanueva, F., García-Lafuente, J., Vargas, J.M., del Río, J., Vázquez, A., Reul, A., Sánchez, A., 2006. Distribution and circulation of water masses in the Gulf of Cadiz from in situ observations. Deep Sea Research II 53, 1144–1160.

Dick, S., Schonfeld, W., 1996. Water transport and mixing in the North Frisian Wadden Sea. Results of numerical investigations. German Journal of Hydrography 48, 27–48.

Dyke, P.P.G., 2001. Coastal and Shelf Sea Modelling. Kluwer, The Netherlands.

Echevarría, F., García-Lafuente, J., Bruno, M., Gorsky, G., Goutx, M., González, N., García, C.M., Gómez, F., Vargas, J.M., Picheral, M., Striby, L., Varela, M., Alonso, J.J., Reul, A., Cozar, A., Prieto, L., Sarhan, T., Plaza, F., Jiménez-Gómez, F., 2002. Physical–biological coupling in the Strait of Gibraltar. Deep Sea Research II 49, 4115–4130.

Elliott, A.J., 1999. Simulations of atmospheric dispersion following a spillage of petroleum at sea. Spill Science and Technology Bulletin 5, 39–50.

Elliott, A.J., Wilkins, B.T., Mansfield, P., 2001. On the disposal of contaminated milk in coastal waters. Marine Pollution Bulletin 42, 927–934.

García-Lafuente, J.M., Cayo-Lucana, N., 1994. Tidal dynamics and associated features of the northwestern shelf of the Alborán Sea. Continental Shelf Research 14, 1–21.

García-Lafuente, J., Delgado, J., Criado-Aldeanueva, F., Bruno, M., del Rfo, J., Vargas, J.M., 2006. Water mass circulation on the continental shelf of the Gulf of Cadiz. Deep Sea Research II 53, 1182–1197.

Gascard, J.C., Richez, C., 1985. Water masses and circulation in the western Alborán Sea and in the Straits of Gibraltar. Progress in Oceanography 15, 157–216.

Gomez-Gesteira, M., Montero, P., Prego, R., Taboada, J.J., Leitao, P., Ruiz-Villareal, M., Neves, R., Perez-Villar, V., 1999. A two-dimensional particle-tracking model for pollution dispersion in A Coruña and Vigo Rias (NW Spain). Oceanologica Acta 22, 167–177.

Harms, I.H., Karcher, M.J., Dethleff, D., 2000. Modelling Siberian river runoff – implications for contaminant transport in the Arctic Ocean. Journal of Marine Systems 27, 95–115.

Havens, H., Luther, M.E., Meyers, S.D., 2009. A coastal prediction system as an event response tool: particle tracking simulations of an anhydrous ammonia spill in Tampa Bay. Marine Pollution Bulletin 58, 1202–1209.

Izquierdo, A., Tejedor, L., Sein, D.V., Backhaus, J.O., Brandt, P., Rubino, A., Kagan, B.A., 2001. Control variability and internal bore evolution in the Strait of Gibraltar: a 2D two-layer model study. Estuarine, Coastal and Shelf Science 53, 637–651.

Jordi, A., Ferrer, M.I., Vizoso, G., Orfila, A., Basterretxea, G., Casas, B., Alvarez, A., Roig, D., Garau, B., Martínez, M., Fernández, V., Fornés, A., Ruiz, M., Fornos, J.J., Balaguer, P., Duarte, C.M., Rodrfguez, I., Alvarez, E., Onken, R., Orfila, P., Tintoré, J., 2006. Scientific management of Mediterranean coastal zone: a hybrid ocean forecasting system for oil spill and search and rescue operations. Marine Pollution Bulletin 53, 361–368.

Kobayashi, T., Otosaka, S., Togawa, O., Hayashi, K., 2007. Development of a non conservative radionuclide dispersion model in the ocean and its application to surface cesium-137 dispersion in the Irish Sea. Journal of Nuclear Science and Technology 44, 238–247.

Korotenko, K.A., Mamedov, R.M., Kontar, A.E., Korotenko, L.A., 2004. Particle-tracking method in the approach for prediction of oil slick transport in the sea: modelling oil pollution resulting from river input. Journal of Marine Systems 48, 159–170.

Kowalick, Z., Murty, T.S., 1993. Numerical Modelling of Ocean Dynamics. World Scientific, Singapore.

Machín, F., Pelegrí, J.L., Marrero-Díaz, A., Laiz, I., Ratsimandresy, A.W., 2006. Near-surface circulation in the southern Gulf of Cadiz. Deep Sea Research II 53, 1161–1181.

Manzella, G.M.R., Elliott, A.J., 1991. EUROSPILL: Mediterranean tidal and residual databases. Marine Pollution Bulletin 22, 553–558.

Mañanes, R., Bruno, M., Alonso, J., Fraguela, B., Tejedor, L., 1998. Non-linear interaction between tidal and subinertial barotropic flows in the Strait of Gibraltar. Oceanologica Acta 21, 33–46.

Mellor, G.L., 2004. User Guide for a Three-dimensional, Primitive Equation, Ocean Model. Princeton University, US.

Nav42, 1998. Report to the Maritime Safety Committee. International Maritime Organization. Available from: <http://www.navcen.uscg.gov/marcomms/imo/document.htm>.

NOAA, 1982. Computer Applications to Tides in the National Ocean Survey. Supplement to Manual of Harmonic Analysis and Prediction of Tides (Special Publication No. 98). National Ocean Service, National Oceanic and Atmospheric Administration, U.S. Department of Commerce, January 1982.

Peliz, A., Dubert, J., Marchesielo, P., Teles-Machado, A., 2007. Surface circulation in the Gulf of Cadiz: model and mean flow structure. Journal of Geophysical Research 112 (C11015), 20.

Periáñez, R., 2005. Modelling the Dispersion of Radionuclides in the Marine Environment. Springer-Verlag, Heidelberg.

Periáñez, R., 2007. Chemical and oil spill rapid response modelling in the Strait of Gibraltar-Alborán Sea. Ecological Modelling 207, 210–222.

Periáñez, R., 2008. A modelling study on ^{137}Cs and ^{239,240}Pu behaviour in the Alborán Sea, western Mediterranean. Journal of Environmental Radioactivity 99, 694–715.

Periáñez, R., 2009. Environmental modelling in the Gulf of Cadiz: heavy metal distributions in water and sediments. Science of the Total Environment 407, 3392–3406.
Periáñez, R., Elliott, A.J., 2002. A particle tracking method for simulating the dispersion of non-conservative radionuclides in coastal waters. Journal of Environmental Radioactivity 58, 13–33.
Periáñez, R., Pascual-Granged, A., 2008. Modelling surface radioactive, chemical and oil spills in the Strait of Gibraltar. Computers & Geosciences 34, 163–180.
Perkins, H., Kinder, T., La Violette, P., 1990. The Atlantic inflow in the western Alborán Sea. Journal of Physical Oceanography 20, 242–263.
Preller, R.H., 1986. A numerical model study of the Alborán Sea gyre. Progress in Oceanography 16, 113–146.
Pugh, D.T., 1987. Tides, Surges and Mean Sea Level. Wiley, Chichester.
Proctor, R., Flather, R.A., Elliott, A.J., 1994. Modelling tides and surface drift in the Arabian Gulf: application to the Gulf oil spill. Continental Shelf Research 14, 531–545.
Riddle, A.M., 1998. The specification of mixing in random walk models for dispersion in the sea. Continental Shelf Research 18, 441–456.
Sannino, G., Bargagli, A., Artale, V., 2002. Numerical modelling of the mean exchange through the Strait of Gibraltar. Journal of Geophysical Research 107 (C8), 3094–3118.
Sannino, G., Bargagli, A., Artale, V., 2004. Numerical modelling of semidiurnal tidal exchange through the Strait of Gibraltar. Journal of Geophysical Research 109, C05011.
Serra, N., Ambar, I., Kase, R.H., 2005. Observations and numerical modelling of the Mediterranean outflow splitting and eddy generation. Deep Sea Research II 52, 383–408.
Schonfeld, W., 1995. Numerical simulation of the dispersion of artificial radionuclides in the English Channel and the North Sea. Journal of Marine Systems 6, 529–544.
Schwiderski, E.W., 1980a. Ocean tides, part 1: global ocean tidal equations. Marine Geodesy 3, 161–217.
Schwiderski, E.W., 1980b. Ocean tides, part 2: a hydrodynamical interpolation model. Marine Geodesy 3, 219–255.
Sotillo, M.G., Alvarez-Fanjul, E., Castanedo, S., Abascal, A.J., Menéndez, J., Emelianov, M., Olivella, R., García-LAdona, E., Ruiz-Villareal, M., Conde, J., Gómez, M., Conde, P., Gutiérrez, A.D., Medina, R., 2008. Towards an operational system for oil spill forecast over Spanish waters: initial developments and implementation test. Marine Pollution Bulletin 56, 686–703.
Tejedor, L., Izquierdo, A., Kagan, B.A., Sein, D.V., 1999. Simulation of the semidiurnal tides in the Strait of Gibraltar. Journal of Geophysical Research 104, 13541–13557.
Tsimplis, M.N., Bryden, H.L., 2000. Estimations of the transports through the Strait of Gibraltar. Deep Sea Research 47, 2219–2242.
Tsimplis, M.N., Proctor, R., Flather, R.A., 1995. A two dimensional tidal model for the Mediterranean Sea. Journal of Geophysical Research 100, 16223–16239.
Vargas-Yáñez, M., Plaza, F., García-Lafuente, J., Sarhan, T., Vargas, J.M., Velez-Belchi, P., 2002. About the seasonal variability of the Alborán Sea circulation. Journal of Marine Systems 35, 229–248.
Werner, F.E., Cantos-Figueroa, A., Parrilla, G., 1988. A sensitivity study of reduced-gravity flows with applications to the Alborán Sea. Journal of Physical Oceanography 18, 373–383.
Yanagi, T., 1999. Coastal Oceanography. Kluwer, The Netherlands.